Research Article | Vol. 29, No. 23 / 8 Nov 2021 / Optics Express 37066

Optics EXPRESS

Active control technology of a diffraction grating wavefront by scanning beam interference lithography

ZHAOWU LIU,[1,5] HANG YANG,[2] YUBO LI,[1,3] SHAN JIANG,[1] WEI WANG,[1] YING SONG,[4] BAYANHESHIG,[1] AND WENHAO LI[1,6]

[1] *Changchun Institute of Optics, Fine Mechanics and Physics, Chinese Academy of Sciences, Changchun Jilin, 130033, China*
[2] *College of Science, Changchun University of Science and Technology, Changchun Jilin, 130022, China*
[3] *Daheng College, University of Chinese Academy of Science, Beijing 101408, China*
[4] *College of Instrumentation and Electrical Engineering, Jilin University, Changchun Jilin, 130061, China*
[5] *zhaowuliu@ciomp.ac.cn*
[6] *liwh@ciomp.ac.cn*

Abstract: To fabricate plain holographic gratings with high wavefront quality and to obtain the wavefront required in varied line-space grating, an active control technology of a diffraction grating wavefront by modulating the phase distribution of the scanning-beam interference lithography system was proposed. Sinusoidal wavefront control is simulated, and the controlled wavefront being almost the same as the target wavefront. A photoresist grating was fabricated whose surface is uniform and the wavefront is ideally sinusoidal. The theoretical analysis and experimental results confirmed that the wavefront of the diffraction grating can be actively controlled by modulating the phase distribution of the scanning-beam interference lithography system.

1. Introduction

The diffraction wavefront is a comprehensive criterion of the grating performance. The diffraction wavefront of the grating directly determines the spectral quality and resolution, and the performance indexes such as stray light and ghost line can be analyzed from the wavefront shape. Therefore, the active control of diffraction wavefront is an important means to improve the grating performance. Such as the pulse compression grating [1,2] which is a core optical element in chirped pulse amplification systems. Research into the control of the wavefront of the diffraction grating is a very important aspect of the chirped pulse amplification systems development process [3–6]. Researchers in the field believe that wavefront distortions increase the far-field divergence angle of the laser beam, broaden the width of the spot, affect directly the focusing properties of the beam, reduce the brightness at the center of the spot and the uniformity of the far-field radiation of the focal spot, and thereby affect the uniformity of the bombardment capsule required of the system and the multi-path transmission in the driver, and even seriously jeopardizing its safe operation. For these reasons, the study of grating diffraction wavefront control has valuable applications in solid-state laser engineering.

In addition, being a core optical element of the planar grating spectrometer [7], the traditional grating, with its straight grooves of equal spacing, has the capability to separate spectra but is unable to provide focusing for spectral imaging. For this reason, a focusing system and an alignment system are needed in the design of the spectrometer. Additional optical components for the spectrometer increase the structural complexity, bulkiness, and inconvenience in use as well as energy losses. In short wave spectrometers such as extreme ultraviolet and soft X-ray [8], substances absorb large amounts of light energy, making the recording of spectral signals

#437593 https://doi.org/10.1364/OE.437593
Journal © 2021 Received 13 Jul 2021; revised 4 Oct 2021; accepted 4 Oct 2021; published 25 Oct 2021

Optics EXPRESS

difficult. In constructing a compact spectrometer having high resolution, strong dispersive power, and high diffraction efficiency, the varied line-space (VLS) grating [9–11] with self-focusing and aberration correction capabilities was developed. By choosing the appropriate fringes distribution of the VLS grating, the focus position and shape of the focal line of the spectrometer can be adjusted to correct the aberration of an optical system, without the optical system used for focusing and collimating. The grating fringe distribution can be expressed by the grating diffraction wavefront. The VLS grating with the required fringe distribution can be manufactured by using the active control technology of a diffraction grating wavefront.

Therefore, wavefront control of the diffraction grating mainly involves two aspects. The first is the control of the wavefront error, which ensures in general that the wavefront is still sufficiently planar. The second is the active control of the wavefront which, for non-planar gratings or variable-pitch gratings, means that the grating has a specific wavefront that can be used in optical systems to compensate for deficiencies of other optical devices.

The scanning beam interference lithography system (SBIL) was first proposed by researchers at the Space Nanotechnology Laboratory of the Massachusetts Institute of Technology(MIT) [12–16]. This system combines the advantages of mechanical scribing, holographic lithography, and laser direct writing [17–21]. Using a small Gaussian beam as a lithographic light source, interference fringes are partially superposed using splicing lithography to obtain a large-size holographic grating. The wavefront of this diffraction grating can be adjusted by controlling the phase distribution of the lithography beam, thereby realizing wavefront control to ensure that it is still an absolute plane, and to obtain the wavefront required for non-planar gratings or variable-pitch gratings.

2. Principle of active wavefront control of a diffraction grating

As shown in the schematic diagram of SBIL(Fig. 1), a small Gaussian laser is separated into two beams as exposure beams and pass through a symmetrically distributed filter for spatial filtering and beam shaping modulation. They are then spread over the upper surface of a grating substrate placed on a two-dimensional stage and superposed at the beam waist. During scanning, the optical path difference of the two beams changes because of disturbances from the external environment. Deviations occur in the positioning of the displacement platform causing shifts in the phase of the interference fringes. These shifts in phase are sent to the phase locking system; subsequently, the phase of the interference fringes is modulated using acousto-optic modulators.

The two lithography beams are superposed at the beam waist to form the same straight periodic fringes as in plane-wave interference. Therefore, the lithography beam can be regarded as plane light with a Gaussian profile. The electric field distribution of the left and right beams can be written as:

$$E_1(x,y) = A_1 e^{-(x^2+y^2+z^2)/w_1^2} e^{j((x-x_d)k\sin\theta + zk\sin\theta - kL_1 + \varphi_0 + \omega_1 t)}\hat{y} \tag{1}$$

$$E_2(x,y) = A_2 e^{-(x^2+y^2+z^2)/w_2^2} e^{j(-(x-x_d)k\sin\theta + zk\sin\theta - kL_2 + \varphi_0 + \omega_2 t)}\hat{y} \tag{2}$$

where A_1 and A_2 denote the energy constant of the two lithography beams, w_1 and w_2 denote the radius of the spot of the two lithography beams at the position of the interference field, x_d denote the positioning error of the displacement platform, θ is the incident angle of the exposure beam, ω_1 and ω_2 denote the angular frequencies of the left and right beams after modulation, L_1 and L_2 the optical path lengths of the left and right beams from the beam splitting grating to the lithography area, and φ_0 denotes the phase constant of the beam after the beam splitting grating. With λ the wavelength of laser beam, its wavenumber is k=2π/λ.

The small difference between the light spots of the left and right exposure beams has a small impact on the exposure contrast and has no impact on the phase of the interference fringes. Therefore, assuming that the two light spots have the same radius, that is, w_1=w_2=w. The incident angle of the exposure beam is θ, and the spot on the substrate surface is elliptical. The semimajor

Optics EXPRESS

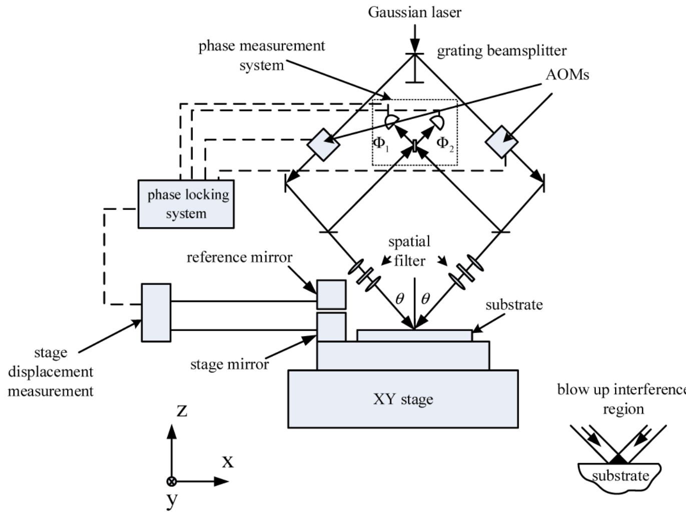

Fig. 1. Schematic diagram of the scanning beam interference lithography system [22].

axis becomes $w/\cos\theta$, along the X direction. The semiminor axis is still w, along the Y direction. Assuming that the grating base surface z = 0, the light intensity distribution after the coherent superposition of the two beams can be written as [23]:

$$I(x,y) = A\exp\left[-2\left(\frac{x^2}{(w/\cos\theta)^2}+\frac{y^2}{w^2}\right)\right]\left[1+\gamma_0\cos\left(\frac{2\pi}{p}x+\varphi_n(x,y)\right)\right] \tag{3}$$

where

$$\begin{cases} A = \sqrt{\varepsilon/\mu}(A_1^2+A_2^2)/2 \\ \gamma_0 = 2A_1A_2/A \\ p = \lambda/2\sin\theta \\ \varphi_n(x,y) = 2\pi\left(-x_d/p+(L_2-L_1)/\lambda+\int(f_1-f_2)dt\right) \end{cases}. \tag{4}$$

In which p is the interference fringe period, γ_0 represents the contrast of interference fringes, and $\varphi_n(x,y)$ denotes the distribution in phase shifts for the interference fringes after the coherent superposition of the two beams from that for an ideal phase of a plane diffraction grating. Controllable by the scanning lithography system, it is called the phase preset. x_d/p measured by the stage displacement measurement system, $(L_2\text{-}L_1)/\lambda$ measured by the phase measurement system and $(f_1\text{-}f_2)$ can be modulated by the phase locking system.

In lithography, the two-dimensional stage scans along the Y direction, which is parallel to the direction of the interference fringe, and scans with speed v. After the scan is completed, the two-dimensional displacement platform steps in the X direction, which is perpendicular to the interference fringe direction, and then continues to scan along the Y direction. The exposure of the upper surface of the substrate can be written as the integral in time of the light intensity distribution after the coherent superposition of two beams, the exposure of the n-th scan can be written as:

$$D_n(x,y) = \int_{-\infty}^{+\infty} I_n(x,y)dt = \frac{1}{v}\int_{-\infty}^{+\infty} I(x,y)dy = A_{Dn}(x,y)\left[1+\gamma_0\cos\left(\frac{2\pi}{p}x+\varphi_n(x,y)\right)\right] \tag{5}$$

Optics EXPRESS

where

$$A_{Dn}(x,y) = A\frac{w}{v}\sqrt{\frac{\pi}{2}}\exp\left\{-2\frac{[x-(n-1)S]^2}{(w/\cos\theta)^2}\right\}, \tag{6}$$

in which S denotes the step displacement between adjacent scans. Repeat the process of "scanning exposure - stepping" repeatedly. If the exposure of the whole grating is completed after N scanning exposures, the exposure of photoresist on the upper surface of the grating substrate is the sum of the exposure of N tracing exposures, expressed as:

$$\begin{aligned} D(x,y) &= \sum_{n=1}^{N} D_n(x,y) \\ &= D_B(x)\left[1+\frac{D_A(x,y)}{D_B(x,y)}\cos\left(\frac{2\pi}{p}x+\Phi_e(x,y)\right)\right] \end{aligned}. \tag{7}$$

In particular, we have

$$\begin{cases} D_B(x,y) = \sum\limits_{n=1}^{N} A_{Dn}(x,y) \\ D_A(x,y) = \gamma_0\sqrt{\left[\sum\limits_{n=1}^{N} A_{Dn}(x,y)\cos\varphi_n(x,y)\right]^2 + \left[\sum\limits_{n=1}^{N} A_{Dn}(x,y)\sin\varphi_n(x,y)\right]^2} \\ \tan\Phi_e(x,y) = \sum\limits_{n=1}^{N} A_{Dn}(x,y)\sin\varphi_n(x,y) / \sum\limits_{n=1}^{N} A_{Dn}(x,y)\cos\varphi_n(x,y) \end{cases} \tag{8}$$

where $2\pi x/p+\Phi_e(x,y)$ represents the total phase distribution after all N scans, and Φ_e denotes the difference in the phase distribution between the grating and the ideal holographic planar grating, knowing that the wavefront of the diffraction grating deviates from that for an ideal plane by $\Phi_e m\lambda/2\pi$, m is the diffraction order. This means that we need only change Φ_e to control the wavefront.

Combining Eq. (3) with the third expression of Eq. (8), we find from the y-direction displacement that the platform moves continuously, and its phase distribution can also be outputted continuously. For the stepping motion in the x direction, the phase distribution is determined by the weight ratio between the preset phase and the preset phase of the adjacent scans of the nth scan. The edge energy of Gaussian beam is low, the preset phase weight ratio of the adjacent scan is low. Therefore, the phase Φ_e of the center line of this scan is approximately:

$$\tan\Phi_e(x,y) \approx \frac{A_{Dn}(x,y)\sin\varphi_n(x,y)}{A_{Dn}(x,y)\cos\varphi_n(x,y)} = \tan\varphi_n(x,y). \tag{10}$$

That is, $\Phi_e(x,y)\approx\varphi_n(x,y)$. The preset phase of the n-th scan can be approximately regarded as the difference between the lithography phase distribution after the N-th lithographic scan and the phase distribution of the ideal fringe from a holographic plane diffraction grating with a uniform grating pitch. The wavefront of the diffraction grating is controlled via the preset phase φ_n, by modulated (f_1-f_2) using the phase locking system. As an example, to demonstrate our wavefront control process, we performed 10 successive scans and plotted the wavefronts of each (Fig. 2). The blue surface identifies the target wavefront, the blue-green surface highlights the target wavefront for each scan, and the red curve gives the contribution of the target wavefront from each scan. Each contribution follows a Gaussian distribution; the ratio increases and decreases slowly between two successive scans, ensuring a smooth transition for the controlled wavefront. A comparison of the controlled wavefront with the target wavefront is shown in Fig. 3(a). Again, the blue surface is the target wavefront, and the blue-green surface is the target wavefront for each scan. The target wavefront basically matches the control wavefront; their difference is presented

Optics EXPRESS

in Fig. 3(b). Except where no splicing occurs between the first two ends of the lithography process, the difference between the target wavefront and the controlled wavefront is almost zero, demonstrating the control of the wavefront of a diffraction grating.

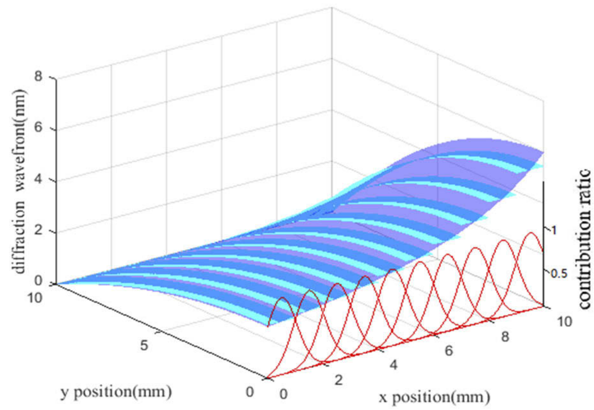

Fig. 2. Control of the wavefront of a diffraction grating.

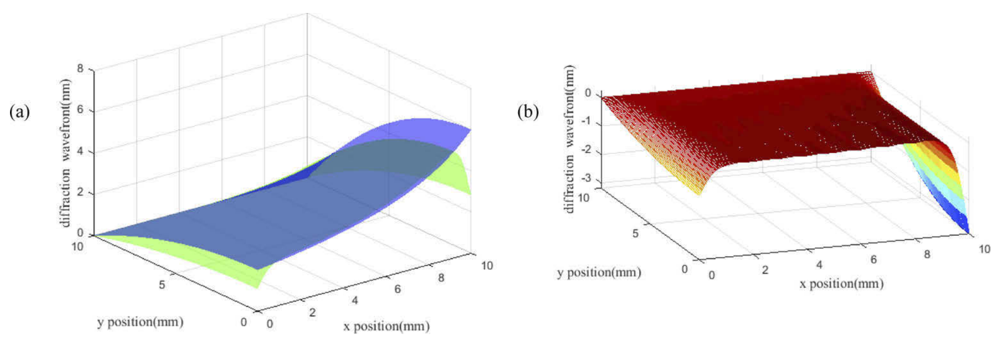

Fig. 3. Comparison of the controlled and target wavefronts: (a) overlay of the controlled and target wavefronts, and (b) difference between the controlled and target wavefronts.

3. Simulation analysis and experimental verification

From the above analysis, any wavefront shape can be adjusted by controlling the preset phase $\varphi_n(x,y)$ during the lithography process. The analysis of the simulation was consistent with actual lithography parameter values. The density of the mask for a plane holographic grating is 1800 gr/mm, and the radius of the beam waist at the substrate is w=0.9 mm. In our study, a step displacement of S=0.6 mm was chosen; with the number of steps being N=134, the size of the grating was then 80 mm×80 mm. Because the Y-direction scan is a continuous lithographic process, we took as an example the control of the vertical fringe direction phase to clarify the process. Specifically, the preset phase of each scan in the Y direction is a constant value and is set to $\Phi_e(x,y)=\pi\sin(2\pi x/L)$, and the target wavefront is $\Phi_e m\lambda/2\pi$, where L=80 mm. Setting m=1, λ=632.8 nm, the target wavefront of the simulated grating (Fig. 4) is sinusoidal with a photovoltaic value of one wavelength.

From Eq. (10), with $\varphi_n(x,y)$ replacing $\Phi_e(\mathrm{x,y})$ in the control system, the preset phase of the n-th scan becomes $\varphi_n(x,y)=\pi\sin[2\pi(n-1)S/L]$. After the N-th scan, with N=134, the simulated control wavefront (Fig. 5) was compared with the simulated grating target wavefront (Fig. 4).

Optics EXPRESS

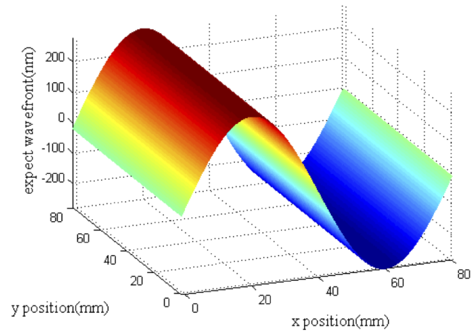

Fig. 4. Simulated grating target wavefront

The difference between the two wavefronts (Fig. 6) is almost zero except for the parts of the lithography process where no superposition occurs—the edges segments of the diffraction grating. In the actual fabrication of the grating, the initial and final positions of scanning can be placed outside the active grating base to eliminate the uncontrollable influences from the edges of the grating. After removing these large differences (see Fig. 7), the wavefront in the Y direction does not change, ensuring the observations are clearer. In a fine scanning of the difference in the wavefronts in the X direction, we find the difference between the control wavefront of the lithography part and the target wavefront of the grating is no more than 0.2 nm and hence can be neglected.

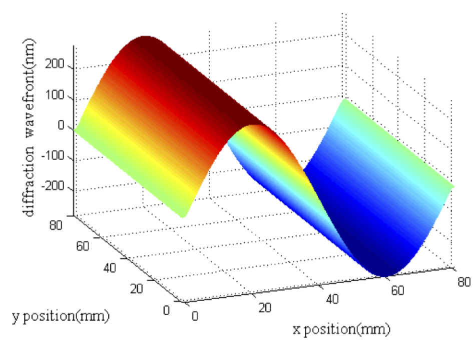

Fig. 5. Simulated grating control wavefront.

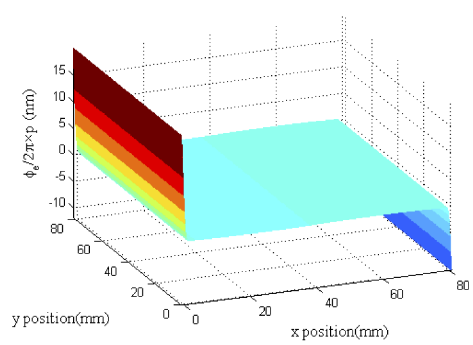

Fig. 6. Difference between the target and control wavefronts for a simulated grating.

Optics EXPRESS

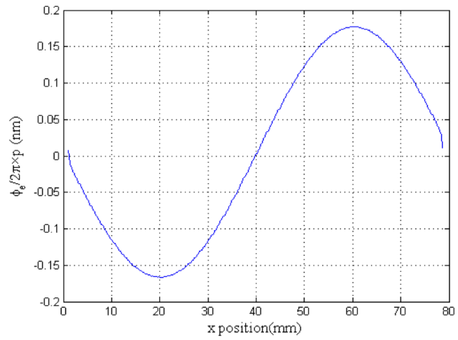

Fig. 7. The wavefront in the Y direction after removing the large differences of Fig. 6.

To verify the results of the theoretical calculations and simulations of wavefront control of a diffraction grating, relevant verification experiments were performed on a prototype of the SBIL system. In regard to settings, the wavelength of the laser light source is 413.1 nm, the laser output power 40 mW, and the scanning and stepping speeds of the displacement platform are 7 mm/s and 1 mm/s, respectively. Light exposures were controlled, and the lithography interference fringes were recorded on a Shipley S1805 photoresist to fabricate the diffraction photoresist grating. The target wavefront of the grating is the same as the sinusoidal wavefront in simulations. The surface of the exposed photoresist grating (Fig. 8) is uniform, it does not change significantly from the wavefront modulation. We used an interferometer (Zygo Corp., Middlefield, CT) to determine the wavefront of the diffraction photoresist grating. Under the influence of the target wavefront, the controlled wavefront (Fig. 9) is seen to have a relatively ideal sinusoidal shape.

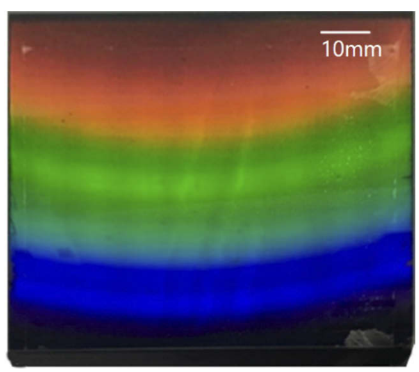

Fig. 8. Photo of the lithography photoresist grating.

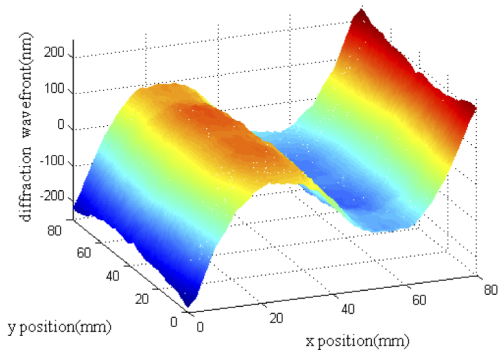

Fig. 9. Control wavefront resulting from the target wavefront of the grating.

4. Conclusion

A method was proposed for the active control of the diffraction grating wavefront using a SBIL system. The phase distribution of the plane grating directly reflects the wavefront of the diffraction grating. SBIL uses a small Gaussian beam as a lithography light source, whose frequency can be modulated by the acousto-optic modulator of the phase-locked system. Presetting the phase distribution resolves the problem of controlling the wavefront of the diffraction grating.

With an 80 mm × 80 mm photoresist grating in simulations, the photovoltaic value of the target wavefront of the grating was sinusoidal. The controlled wavefront was almost the same as the target wavefront of the grating, except for the edges. The difference between the target wavefront and the diffraction wavefront is no more than 0.2 nm and hence can be neglected.

In experiments to fabricate this grating, the target wavefront of the grating was the same as in the simulation, The edges of the grating base were placed outside the scanning area to eliminate their uncontrollable influences. The surface of the photoresist grating was uniform, and does not vary significantly under wavefront modulation. The diffraction wavefront of this photoresist grating was recorded using an interferometer. The control wavefront was relatively sinusoidal, proving that by the scanning exposure system the main wavefront of the grating can be modulated by the phase distribution of the plane grating fringe and that the method of dynamic control is effective.

Funding. National Natural Science Foundation of China (61905243, 61905245); Jilin Province Science & Technology Development Program Project in China (20190303019SF, 20200401071GX); R & D projects in key areas of Guangdong Province (2019B010144001).

Acknowledgment. We thank Ying Song from Jilin University for developing the control system and Hang Yang from Changchun University of Science and Technology for helping with the experiment.

Disclosures. The authors declare that there are no conflicts of interest related to this paper.

Data availability. Data underlying the results presented in this paper are not publicly available at this time but may be obtained from the authors upon reasonable request.

References

1. Z. Qiu, M. Wang, P. U. Yunti, and M. A. Ping, "Investigation progress of laser damage properties on multilayer dielectric film pulse compression grating," Journal of Materials Science and Engineering **35**(2), 329–338 (2017).
2. T. Dietrich, S. Piehler, C. Rcker, M. Rumpel, and T. Graf, "Passive compensation of the misalignment instability caused by air convection in thin-disk lasers," Opt. Lett. **42**(17), 3263–3266 (2017).
3. S. Zhang, J. Zhang, Y. Zhou, X. Wang, B. Deng, J. Su, and D. Hu, "Influence of wavefront distortion on spatial-temporal property of laser pulse output by grating compressor," Chin. J. Laser **45**(04), 0401011 (2018).
4. D. Zhao, X. Wang, J. Mu, Y. L. Zuo, and Q. H. Zhu, "Effect of grating groove density error on the output pulses of the tiled grating compressor and corresponding compensation scheme," Acta Phys. Sin. **66**(2), 024201 (2017).
5. X. Huang, D. Hu, Z. Wei, W. Dai, and J. Feng, "Optical zooming based on focusing grating in direct drive ICF," Opt. Express **24**(19), 22051–22060 (2016).

6. H. Li, G. Liang, and Y. Huang, "An efficient radiation analysis approach through compressive model for laser driven inertial confinement fusion," Comput. Phys. Commun. **259**, 107644 (2021).
7. M. Chi, X. Han, Y. Xu, H. Xing, Y. Liu, and Y. Wu, "Micro two-dimensional slit-array for super resolution beyond pixel Nyquist limits in grating spectrometers," Opt. Express **29**(9), 13669–13680 (2021).
8. W. Li, Y. Jiang, N. Wu, T. Zhang, and K. Wang, "Analysis for groove density and spectral resolution of varied-line-space gratings in EUV spectrum," Chin. J. Lumin. **36**(9), 1094–1099 (2015).
9. J. Chen, W. Chen, G. Zhang, H. Lin, and S.-C. Chen, "High-resolution compact spectrometer based on a custom-printed varied-line-spacing concave blazed grating," Opt. Express **25**(11), 12446–12454 (2017).
10. A. N. Shatokhin, A. O. Kolesnikov, P. V. Sasorov, E. A. Vishnyakov, and E. N. Ragozin, "High-resolution stigmatic spectrograph for a wavelength range of 12.5–30 nm," Opt. Express **26**(15), 19009–19019 (2018).
11. Y. Shimizu, R. Ishizuka, K. Mano, Y. Kanda, and W. Gao, "An absolute surface encoder with a planar scale grating of variable periods," Precis. Eng. **67**, 36–47 (2021).
12. P. T. Konkola, "Design and analysis of a scanning beam interference lithography system for patterning gratings with nanometer-level distortions," Ph.D. thesis (Massachusetts Institute of Technology, 2003).
13. C. G. Chen, "Beam alignment and image metrology for scanning beam interference lithography fabricating gratings with nano-meter phase accuracy," Ph.D. thesis (Massachusetts Institute of Technology, 2003).
14. C. G. Chen, P. T. Konkola, R. K. Heilmann, G. S. Pati, and M. L. Schattenburg, "Image metrology and system controls for scanning beam interference lithography," J. Vac. Sci. Technol. B **19**(6), 2335–2341 (2001).
15. J. Montoya, "Toward nano-accuracy in scanning beam interference lithography," Ph.D. thesis (Massachusetts Institute of Technology, 2006).
16. R. K. Heilmann, P. T. Konkola, C. G. Chen, G. S. Pati, and M. L. Schattenburg, "Digital heterodyne interference fringe control system," J. Vac. Sci. Technol. B **19**(6), 2342–2346 (2001).
17. Y. Zhu, L. Wang, M. Zhang, S. Lu, K. Yang, and C. Hu, "Novel homodyne frequency-shifting interference pattern locking system," Chin. Opt. Lett. **14**(6), 41–46 (2016).
18. D. Ma, Y. Zhao, and L. Zeng, "Achieving unlimited recording length in interference lithography via road-beam scanning exposure with self-referencing alignment," Sci. Rep. **7**(1), 926 (2017).
19. Z. Liu, S. Jiang, X. Li, Y. Song, W. Li, and Bayanheshig, "Precision measurement of X-axis stage mirror profile in scanning beam interference lithography by three-probe system based on bidirectional integration model," Opt. Express **25**(9), 10312–10321 (2017).
20. S. Jiang, B. Lü, Y. Song, Z. Liu, W. Wang, L. Shuo, and Bayanheshig, "Heterodyne period measurement in a scanning beam interference lithography system," Appl. Opt. **59**(19), 5830–5836 (2020).
21. Y. Song, Y. Liu, S. Jiang, Y. Zhu, L. Zhang, and Z. Liu, "Method for exposure dose monitoring and control in scanning beam interference lithography," Appl. Opt. **60**(10), 2767–2774 (2021).
22. Y. Song, "Research on the interference fringe static and dynamic phase-locking technology in the lithography system of the holographic grating," Ph.D. thesis (Chinese Academy of Sciences, 2014), p. 54.
23. S. Jiang, "Study on measurement and adjustment of interference fringes for scanning beam interference lithography system," Ph.D. thesis (Chinese Academy of Sciences, 2015), p. 65.